Experimental and Theoretical Studies on the Dynamic Characteristics During Speed Down of Inverter Heat Pump

Yoon Jei Hwang* and Ho Young Kim**

Key words : Variable speed heat pump, Inverter driven, Scroll compressor, Transient, Capillary tube, Cycle simulation, Driving frequency

Abstract

A series of tests were performed to verify the transient characteristics of heat pump in heating and cooling mode when operating speed was varied over the 30 to 102Hz. One of the major issues that has not been addressed so far is transient characteristics during speed modulation. The model for cycle simulation has been developed to predict the cycle performance under conditions of decreasing drive frequency and the results of the theoretical study were compared with the results of the experimental study. The simulated results were in good agreement with the experimental result within 10%. The transient cycle migration of the liquid state refrigerant causes significant dynamic change in system. Thus, the migration of refrigerant was the most important factor whenever do experimental results analysis or develop simulation model.

Nomenclature

A : heat transfer area [㎡]
d : tube diameter [mm]
H : enthalpy [kJ/kg]
h : heat transfer coefficient [W/㎡ K]
$\dot{m}$: mass flow rate of refrigerant [kg/h]
m : mass [kg]
Q : heat capacity [W]
t : time
T : temperature [℃]
U : overall heat transfer coefficient [W/㎡K]
V : volume [㎥]
x : length [m/quality]
Z : flow direction
v : specific volume [㎥/kg]
: density [kg/㎥]
Γ : conversion factor(=1/427kcal/kgm)

* Digital Appliance Research Laboratory, LG Electronics Inc., Seoul, Korea
** Department of Mechanical Engineering, Korea University, Seoul, Korea

1. Introduction

A system with a variable speed compressor is becoming more beneficial because it can respond properly to outdoor loads. It is called a variable-speed or modulating heat pump which operates on cooling or heating mode by changing the speed of the compressor using an inverter circuit. In most previous works on unsteady state cycle modeling, the temperature variations caused by the irregular migration of refrigerant during start up or shutdown are experimented or predicted[(1)~(3)]. For the system using a variable speed compressor, however, it is necessary to develop a simulation model that predicts the transient state of the cycle during the change of compressor driving frequency. The simulation model can reflect on the design of the system by analyzing the properties and behaviors of refrigerant according to time. Even though there have been many studies, studies on unsteady state behaviors are conducted by only a few researchers. Matsuoka, et al[(4)] tried out the opening control of electric expansion valve(EEV) in order to correspond to the dynamic characteristics. They obtained the step response waves from the superheat response with varying the compressor frequency, the speed of indoor fan or the opening of EEV. In the study, good results are obtained by applying preview tracking control algorithm to a refrigeration cycle. In order to control the dynamic characteristics, the gain was obtained from compressor speed as input signal and the corresponding opening as operator. Yasuda, et al[(5)] made transfer function model consisted of nonlinear equation using characteristics values and parameters that affect refrigeration system. The EEV opening using PI controlled the superheat at evaporator outlet. In consequence, it is essential to clarify the characteristics during speed changing by experiments and simulation models for various conditions. Therefore, the purpose of this study is to develop a systematic design process and a design program of variable-speed heat pump cycle through analyzing the transient characteristics of the cycle during a compressor speed change.

2. Experimental Set Up and Procedure

A cycle can be optimized through improving efficiency of each major component such as designing heat exchanger pass, improving efficiency of distributor, modifying length and diameter of capillary tube, changing refrigerant.

In Fig.1, (P) is a pressure measuring point, (T) is a temperature measuring point, (W) electric consumption, (G) air flow rate, (H) enthalpy, (Q) capacity, and (FM) is a mass flow rate measuring point. To explain briefly about the test procedures, after two minutes from steady, desired drive frequency was set and the unsteady state data were stored in a file every 5-second. The measuring points consist of 24 temperature, 2 pressure and 1 mass flow rate signals, and also the capacity, compressor electric input, and airflow rate can be measured.

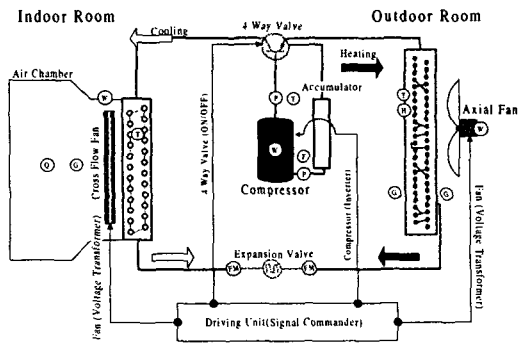

Fig. 1 Schematic diagram of the system unit set up.

Because all the instruments are open to the noise from the inverter driver, the count circuit for reducing the noise is needed. Grounding or filtering using an electrolysis condenser can solve the problem. In this experiment, the mass flow meter and compressor inlet and outlet were wound with grounding copper wire, and thermocouples and pressure gauge lines were filtered with 103~104pF capacity electrolysis condensers attached to each channel of instrument. The specification of the system of this experiment is shown in Table 1.

3. Experimental Results

The suction and discharge pressure variations as a function of time during speed down are shown in Fig.2. When the compressor speed decreases, there is a little change of pressure because the only small amount of liquid refrigerant flows into the compressor and evaporates. It is somewhat different from the frequency increasing case, which is occurred sudden increase of pressure. From the visualization tests, sudden flooding could not be observed in the compressor. In all cases of speed down, the effect of changing magnitude of speed on system dynamics become smaller than that of speed up. From these results, the high and low side pressure was changed symmetrically without

Table 1 Specification of heat pump system

Component	Specification	Unit
Cycle	Capacity : 3570(C)/4300(H)	kcal/h
	Power :1455(C)/1700(H)	W
	Refrigeration : Oil4GS	
	Charging Amount : 850	g
	Dehumidification : 2.3	l/h
Compressor	Type : High Side Scroll	
	Stroke Volume : 15.6	㎥/rev.
	Frequency : 30~110	Hz
	Power : 1Φ-200V-60Hz	
Indoor Unit	Air Flow Rate:10.0(C)/10.5(H)	㎥/min.
	Fan Type : Cross Flow	
	Size : 880 x 302 x 183	mm
	Type : 2Row-2Pass-12Step	
Outdoor Unit	Air Flow Rate:26.4(C)/28.3(H)	㎥/min.
	Fan Type : Axial	
	Size : 800 x 530 x 270	mm
	Type : 2Row-4Pass-24Step	
Expansion Device	Diameter : 1.7~1.9	mm
	Length : 1000~1100	mm

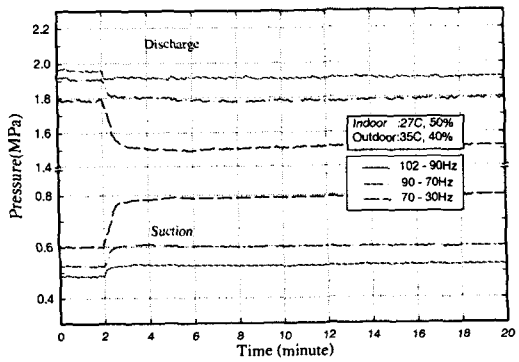

Fig. 2 Measured refrigerant pressure under drop down frequency conditions in cooling mode.

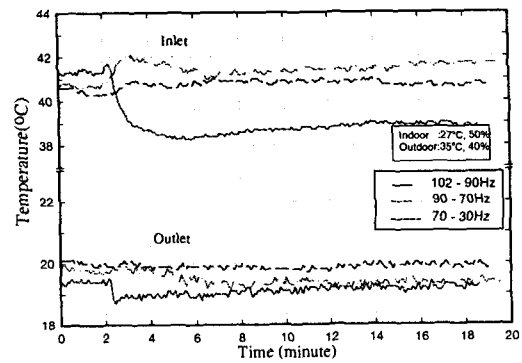

Fig. 3 Measured refrigerant temperature at capillary inlet and outlet under drop down frequency conditions in cooling mode.

sudden change of low side pressure if there was no dynamics of liquid refrigerant flow.

Figure 3 shows the temperature variations of the capillary tube inlet and outlet as a function of time during speed down. The inlet temperature decreases quickly as drive frequency decreases at 70 to 30Hz. But in other cases, it maintained its temperature after slight increase. In the case of 70 to 30Hz, the state point of the capillary inlet moved downward walk along near liquid saturation line to keep subcooling state. It was caused by the mass flow rate and condensing pressure decreased greatly at the same time. In the case of 102 to 90Hz as well as 90Hz to 30Hz, the temperature of capillary outlet increased because of reduced pressure difference causing the rise of evaporating pressure by decreased compressor frequency and then it decreased slowly to back up subcooling while keeping same pressure difference. The temperature of capillary inlet increased after change and then decreased slowly. That is because of the decreased subcooling caused by decreased condensing pressure and mass flow rate due to decreased compressor frequency.

Figure 4 shows the evaporating and condensing temperature variations as a function of time during speed down at heating condition. The condensing temperature decreases after change, but the evaporating temperature, which is the average of 4 passes, takes more time to reach steady state in case of decreasing frequency from 70 to 30Hz. Generally, the possibility of frosting increases when the relative humidity is over 70% and the air temperature is below 5℃. For an R-22 refrigerant, if the air temperature is below 5℃, the evaporating temperature is less than 0℃ satisfying Eq.(1). The frosting in evaporator occurs under the following conditions:

$$T_p < T_{dew} \text{ and } T_p < 0\,℃$$
$$T_{dew} = f(T_{db}, RH) \quad (1)$$

However, this result shows that the evaporating temperature remain constant while it below 0℃. In this experiment, frost can be seen partly because the refrigerant mass flow rates in each pass are different due to poor distribution.

4. Simulation Model

A numerical analysis model is developed to predict the transient state characteristics of the system during compressor speed changes using the analysis modeling of each major component as follows.

4.1 Compressor

After the refrigerant gas flows into the scroll compressor shell and the outside pocket, the compression process takes place as the rotating scroll moves the gas inward while the crank angle increases. Then the compressed gas is discharged through the discharge port of the fixed scroll. The energy and mass conservation equations and vapor state equations are applied for this compression process. The temperature variation equation of the refrigerant is driven from the energy and mass conservation equations. The pressure variation equation is obtained from the actual vapor state equation. The equation for refrigerant mass flow rate according to the compressor speed is also additionally needed for an unsteady state modeling. The temperature variation equation driven from the 1st law of thermodynamic is differentiated on time and can be expressed by mass and volume rates as follows:

$$\frac{dT}{dt} = \frac{\dot{Q} + \sum (H_i - H)\frac{dm_i}{dt} - \left(\frac{dV}{dt} - V\frac{dm}{dt}\right)\left\{\left(\frac{\partial H}{\partial V}\right)_T - \frac{\partial P}{\partial V}\right\}_T \cdot V}{m\left[\left(\frac{\partial H}{\partial T}\right)_V - \frac{\partial P}{\partial T}\right]_V \cdot V} \quad (2)$$

The volume change can be calculated from the volume curve according to the rotated angle using geometrical equations, and the mass flow rate in the volume of scroll can be expressed as follows:

$$\frac{dm_i}{dt} = \frac{dm_o}{dt} + \frac{dm}{dt} \tag{3}$$

The equation for pressure changes on time can be obtained from the state equation differentiated on time as follows:

$$\frac{dP}{dt} = P\left\{\frac{1}{m}\frac{dm}{dt} + \frac{1}{T}\frac{dT}{dt} - \frac{1}{V}\frac{dV}{dt}\right\} \tag{4}$$

4.2 Heat exchangers

The heat exchangers used in this experiment and modeling are pinned tube type coils that exchange heat between the refrigerant in the tube and the air passing through the pins and tubes. Because the heat exchanger can serve as a condenser or an evaporator depending on the operational purpose, there is not a great difference in developing a calculation model for both. However, it is necessary to consider the latent heat for the calculation of evaporator on the airside and the sub-cooling refrigerant in the condenser. Modifying the lumped parameter model proposed by MacArthur[6], the cycle model by Domanski & Didion[7], and EVSIMM subprograms of Domanski[8], a simulation model for heat exchangers is developed. The following unsteady discrete equation in terms of enthalpy differences can be achieved after multiplying with the expanded unsteady 1st order continuity equation and energy equation with neglected momentum terms:

$$(H_i' - H_i^o)\frac{\rho_i^o V_i^o}{\Delta t} = \dot{m}_j'(H_i' - H_j') + \dot{m}_{j-1}'(H_{j-1}' - H_i') + (UA)_i(T_{air,i}' - T_{ref,i}') \tag{5}$$

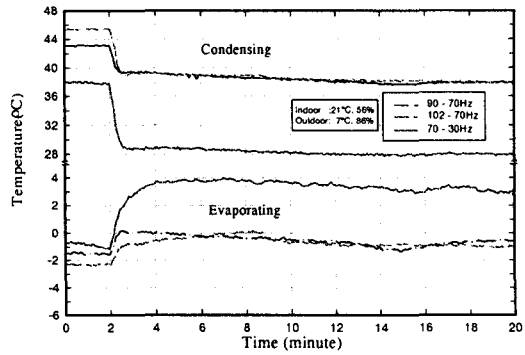

Fig. 4 Measured refrigerant temperature at indoor and outdoor heat exchanger under drop down frequency conditions in heating mode.

An upwind scheme is used because there should not be a false diffusion error. That is because the diffusion term can be ignored due to the great influence of convection heat transfer of the refrigerant flow. Because of the great effect of upstream, the unsteady term is evaluated using a fully implicit scheme that takes j-1 value to calculate the point i., and the energy equation for refrigerant can be written as follows:

$$a_P\varphi_P = a_E\varphi_E + a_W\varphi_W + S \tag{6}$$

where

$$a_p = a_E + a_W = [[\dot{m}_{j-1}', 0]] + [[\dot{m}_j', 0]] + \frac{\dot{\rho_i} V_i}{\Delta t}$$

$$S = -(UA)_i(T_{air,i}' - T_{ref,i}') + \frac{\rho_i^o V_i}{\Delta t} H_i^o$$

The same method can be applied to the grid point i, and the equation for the air temperature can be derived as follows:

$$T_{air,i}' = \frac{(G_a c_{p,a})T_{air,i+1}' + (UA)_i T_{ref,i}' + \frac{(G_a c_{p,a})_i}{\Delta t} T_{air,i}^o}{\frac{(G_a c_{p,a})_i}{\Delta t} + (G_a c_{p,a}) + (UA)_i} \tag{7}$$

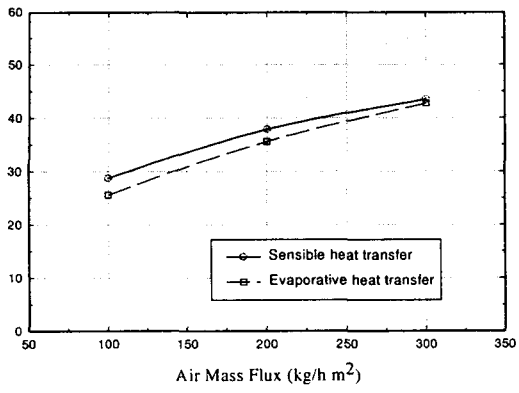

Fig. 5 Experimental heat transfer coefficient in the indoor unit versus mass flux for 2 Row, 19Fpi.

In a heat exchanger model simulation, the correlation of the heat transfer coefficient, the pressure drop of the refrigerant and the airside heat transfer are necessary in order to find the overall heat transfer coefficient U in Eq.6 and 7. However, a different heat transfer coefficient should be used for the different state of the refrigerant because the refrigerant in a heat exchanger exists as single phase state, liquid or vapor, or as two-phase state depending on cooling and heating mode conditions and the compressor driving frequency. Because the heat resistance of air is over 70% of the total resistance (1/UA), the properties of air are great factors on model calculation. McQuiston, Nakayama, Gray and Webb, and Nagaka[9] presented general equations on finned tube exchangers with flat fins and enhanced fins. However, because the shapes of pins are various and the airflow passing the fin is very complicate, the estimation of the exact heat transfer of air is very difficult. Since the fin, Φ7-LG, used in this experiment has also an unique shape and arrangement, the correlation with the experimental heat transfer coefficient is used rather than the theoretical correlation. Figure 5 shows the experimental heat transfer coefficient of air for the indoor unit.

4.3 Expansion device

The expansion device model used in this study is based on the idea of the pressure drop due to the friction and the mass flow rate control according to the characteristics of Fanno flow proposed by Domanski[7]. Though the refrigerant at the capillary tube entrance is sub-cooled and mostly passing the saturated liquid line, it is necessary to consider two-phase flow because there could be no more sub-cooled liquid at the instant when the mass flow rate changes with the changed compressor driving frequency. If the saturated temperature at the condenser outlet pressure is lower than the entrance temperature, the calculation for two-phase flow should be made, and if it is higher the calculation at the entrance should be made for sub-cooling region. The capillary tube simulation model for cooling and heating mode is a simple linear model without the consideration of thermodynamically non-equilibrium effect assuming that the flow is one-dimensional and adiabatic and the friction has a great effect on the pressure drop. The momentum equation from the governing equation for control volume is shown in Eq.8, and the energy equation is shown in Eq.9.

$$\left(\frac{A}{\dot{m}_r}\right)^2 \int_{P_i}^{P_{i-1}} \rho dp + \frac{2}{d_{ci}} \int_{Z_i}^{Z_{i-1}} f dZ + \ln \frac{\rho_i}{\rho_{i+1}} = 0 \qquad (8)$$

$$H + \Gamma \cdot \frac{\bar{\omega}^2}{2g_o} = H_{inlet} \qquad (9)$$

To explain briefly on the calculation procedure, first, it is necessary to examine whether choked flow occurs as entropy decreases when

the difference of the entropy at the capillary entrance and the newly calculated entropy is less than zero as the pressure drops. If the flow is not choked, the calculation should be repeated with an increased mass flow rate. If choked, the length of the capillary tube should be checked. If the calculated length of the capillary tube is shorter, then the calculation

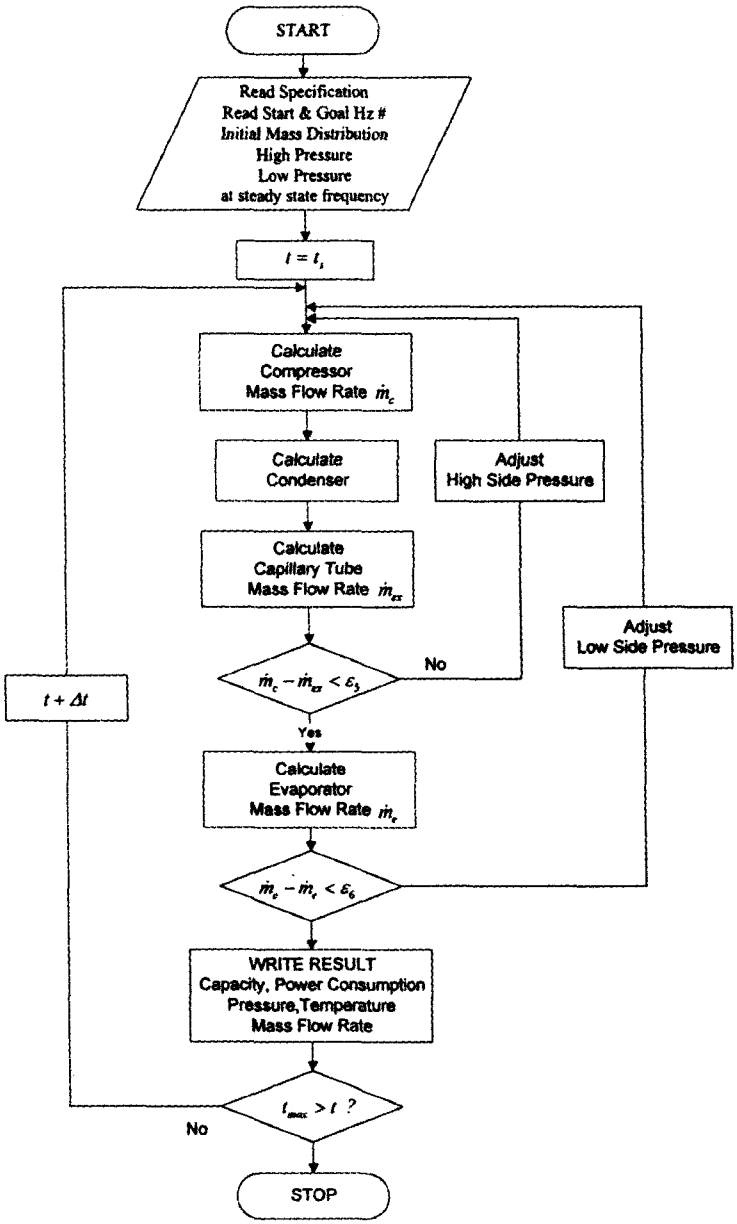

Fig. 6 Flow chart for cycle simulation.

should be done with reduced refrigerant mass flow rate. If the length is longer and the pressure in choked flow is greater than the calculated pressure of the compressor inlet, then the calculation should be made with the increased refrigerant mass flow rate. If the choked flow occurs and the pressure is less than the calculated pressure of the compressor inlet (i.e. the capillary exit conditions), then the quality, pressure, enthalpy, refrigerant mass flow rate should be calculated.

4.4 4-way valve

A four-way valve changes the system from the cooling to the heating mode. There occurs a pressure drop because of the conduction, convection, and radiation heat transfer and also its complex pass structure. According to Nguyen [10], the conduction is the most significant in heat transfer, and the pressure drop increases linearly as the refrigerant mass flow rate increases. Also, he reported that the influence for heating mode is a little greater than that for cooling mode, but ultimately the temperature difference of the two fluids and the mass flux are the main factors. In this study, pressure sensors are attached to inlet and outlet of 4-way valve and the measured data are applied to make the following first-order linear equation.

$$\Delta P = \alpha_1 + \alpha_2 \dot{m}_r / (\alpha_3 + \dot{m}_r) \tag{10}$$

The temperature of suction gas increases due to the conduction heat transfer between two fluids while the exit temperature decreases. The difference between cooling and heating mode can be neglected because the effect of convection and radiation from surrounding is very small. Therefore, the following 1st order linear equations are used.

$$\Delta T_{suc} = \beta_1 \cdot Hz + \beta_2 \tag{11}$$

$$\Delta T_{dis} = \beta_3 \cdot Hz + \beta_4 \tag{12}$$

4.5 Cycle modeling

In this cycle model, the prediction of transient state characteristics during the change of operating frequency is the main purpose. Subprograms were made to show the system change in infinitesimal time using governing equations including unsteady terms for each major component. One of the typical solving methods for an unsteady system is to solve simultaneously the whole governing equations enumerated with dependent variables on infinitesimal time. Because these are one-dimensional differential equations on space or time, the 4th order Runge-Kutta method can be applied. This method has very good convergence, but has a disadvantage of somewhat low accuracy. Therefore, after solving the unsteady state governing equations for each major component separately on infinitesimal time and balancing with the results, the calculation for the next time step was taken orderly in this model. The initial conditions from the steady state refrigerant distribution for each frequency were used. Because the initial conditions influence greatly to the simulation results, the simulation was performed using measured refrigerant property data referring to the related references and experiment in order to obtain precise initial conditions. For liquid or vapor state region, the following Eq.13 is used. For two-phase state, the solutions can be obtained from Eq.14 assuming linear change from the dry bulb temperature 1 to 0 with known temperature and pressure.

$$\rho_{cs} = f(P_d, T_{cg}) \tag{13}$$

Table 2 Initial conditions at typical frequencies

Input Name	Start Frequency	Rotating Speed	Evaporating Pressure	Condensing Pressure	Compressor Surface Temperature
Unit	(Hz)	(rpm)	(MPa)	(MPa)	(℃)
Cooling	90	5400	0.82	1.55	82
Heating	90	5400	0.44	2.04	93

$$m_{c1} = \overline{\rho}_{cs} V_c$$

$$\rho_{cl} = f(P_d, T_{cs}, x) = \rho_g x + \rho_l (1 - x)$$

$$m_{c2} = \int_{x=1}^{x=0} \rho_{cl}(x) \cdot V_c dx \qquad (14)$$

The initial conditions used in this simulation are shown in Table 2. Assuming no slip of motor except high and low frequencies, the system was simulated using saturation temperature from evaporating and condensing pressure. The surface temperature of the compressor varied with operating frequency. However, the steady-state values were used as the initial values since fluctuation was not so great during steady-state operation,. The flow chart of this cycle simulation is shown in Fig.6.

5. Results and Discussion

The variations of capacity, refrigerant mass flow rate, pressures and condensing and evaporating temperature were simulated using a theoretical model when the drive frequency in a steady state was changed to a desired frequency. The theoretical results were compared with the experimental results for 70 Hz. The variations of cooling capacity during sudden decrease of drive frequency from 90Hz to 70, 50, and 30Hz in cooling mode are shown in Fig.7. A cooling capacity was calculated from

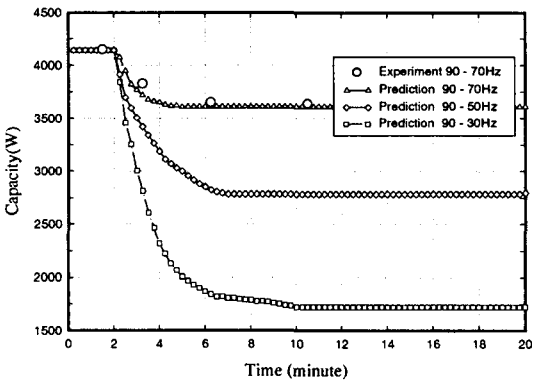

Fig. 7 Calculation results of capacity for various system frequencies according to time under standard cooling condition.

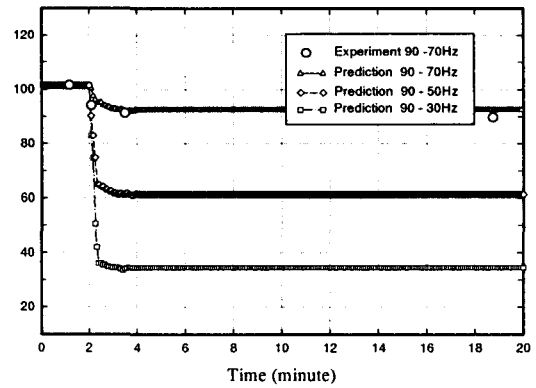

Fig. 8 Calculation results of mass flow rate for various system frequencies according to time under standard cooling condition.

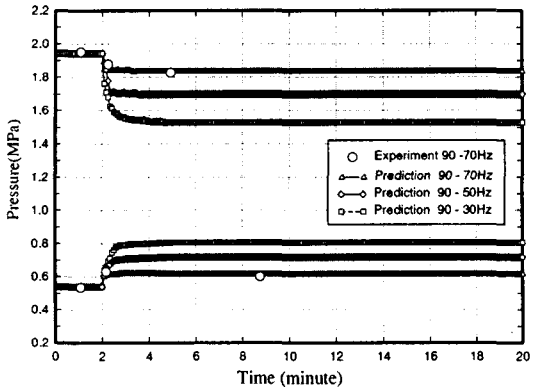

Fig. 9 Calculation results of suction and discharge pressure for various system frequesncies according to time under standard cooling condition.

refrigerant mass flow rates and enthalpy differences between evaporator inlet and outlet. Because the enthalpy differences depend on accuracy of evaporator pressure and temperature, the mass balance and the energy balance should be less than a specified value(ε) in order to predict the cooling capacity precisely. At 70Hz, the simulated values are steeper than experimental data in transient state during the first 6 minutes, but after that, the simulated results coincide relatively well with the experimental ones for all time regions. Heat exchanger model influences capacity calculation because pressure regulation occurred when superheat region in heat exchanger increased during subcooled region decreased. The frequency increase width is proved to be a main factor in the transient state time because it takes more time to reach steady state if the width is greater. The experimental results were obtained from the airside, the steady state was achieved with a rather slow curve because of the slow response of psychro-meter. The calculated results of refrigerant mass flow rate during sudden decrease of drive frequency from 90Hz to 70, 50, and 30Hz in cooling mode are shown in Fig.8. The circulating refrigerant mass flow rates get to the steady value slow except first one minute unlike increasing cases. The larger the decreasing frequency width, the faster the steady state can be achieved. Figure 9 shows the compressor suction and discharge pressure variations during sudden decrease of drive frequency from 90Hz to 70, 50, and 30Hz in cooling mode. As the drive frequency decreases the pressure at the high-pressure side decreases and that of the low pressure side increases. In the case of 70Hz, though the simulation values are a little different from the experimental ones, but the overall variation trend is similar. When the drive frequency is changed from 90 Hz to target value, sudden change of evaporating pressure due to flooding of refrigerant does not occur unlike increasing cases. Suction pressure variation is very similar to all cases, but discharge pressure decrease becomes greater as frequency width decreases.

6. Conclusions

The conclusions of this study were drawn as follows:

(1) During cooling and heating mode, in the case of changing operation condition from high speed to low, the transient influences were moderate because there was no excessive refrigerant flow into compressor from migrated refrigerant and suction pressure drop. The pressure variation of condenser was very similar to that of temperature variation at condenser and compressor outlet different from the case of speed up.

(2) The transient state simulation model for each major component of the cycle system was developed, and the results of the simulation were in good agreement with the experimental ones

within 10% for transient conditions during speed down.

(3) The transient state cycle model was simulated with initial inputs of condensing pressure and evaporating pressure obtained through the experiments of each frequency. From the results it could be drawn that the transient cycle migration of the liquid state refrigerant caused significant dynamic change in system. Therefore, the migration of refrigerant was the most important factor in accuracy for an experimental analysis or development of transient model.

7. Further Studies

Since only standard operation conditions were performed in this study, transient characteristics of system under various indoor and outdoor temperature conditions as well as overload conditions should be defined through further studies. Moreover, studies on transient state characteristics of a system using electric expansion devices should be proceeded in order to maximize the system efficiency in 10~130 Hz operating conditions.

References

(1) Murphy, W. E. and Goldschmidt, V. W., 1985, "Cyclic Characteristics of a Typical Residential Air Conditioner-Modeling of Start-Up Transients", *ASHRAE Transactions*, No.2A, pp. 427-444.

(2) Murphy, W. E. and Goldschmidt, V. W., 1984, "Transient Response of Air Conditi oners-A Qualitative Interpretation Through a Sample Case", *ASHRAE Transactions*, No.1B, pp. 997-1008.

(3) Murphy, W. E. and Goldschmidt, V. W., 1986, "Cycling Characteristics of a Residential Air Conditioner-Modeling of Shutdown Transients", *ASHRAE Transactions*, No.1A., pp. 186-202

(4) F. Matsuoka, H. Nagatomo, 1988, "Dynamic Response and Electrical Control for the Air Conditioner", JAR Transactions, Vol. 5, No.1, pp. 43-54. (in Japanese)

(5) Yasuda, T.,Yanagisawa, T., Izushi, M., 1994, "A dynamic model of a vapor compression refrigeration cycle", JAR *Transactions*, No.3, pp. 263-275. (in Japanese)

(6) MacArthur, J. W. and Grald, E. W., 1989, "Unsteady Compressible Two Phase Flow Model for Predicting Cyclic Heat Pump Performance and a Comparison With Experimental Data", Int. J. of Refrigeration, Vol.12, No.1 , pp. 29-41.

(7) Domanski, P. A. and Didion, D. A., 1983, Computer Modeling of The Vapor Compression Cycle with Constant Flow Area Expansion Device, Report No. NBS Building Science Series 155, NBS.

(8) Domanski, P. A., 1989, EVSIMM-An Evaporator Simulation Model Accounting for Refrigerant and One Dimensional Air Distribution, *NISTIR89-4133*.

(9) McQuiston, F. C., Parker, J. D., 1994, *Heating, Ventilating and Air Conditioning*, 4th Edition, John Wiley & Sons.

(10) Nguyen, H. V., 1986, Reversing valve heat transfer and pressure drop and their effects on the steady-state performance of a heat pump, Ph. D. Dissertation, Purdue University.

(11) Rice, C. K., 1988, Efficiency Characteristics of Speed Modulated Drives at Predicted Torque Conditions for Air-to-Air Heat Pumps, ASHRAE Transactions, DA-88-

(12) Rice, C.K., 1991, The ORNL Modulating Heat Pump Design Tool MODCON-User's Guide, ORNL-CON-343.